Exploiting Synergy Between Ligand Design Effects and Counterion Interactions to Boost Room Temperature Phosphorescence from Luminescent Cu(I) Compounds

Rajarshi Mondal,[a] Issiah B. Lozada,[a] Rebecca L. Davis,[a] J. A. Gareth Williams[b] and David E. Herbert[a*]*

[a]Department of Chemistry and the Manitoba Institute for Materials, University of Manitoba, 144 Dysart Road, Winnipeg, Manitoba, R3T 2N2, Canada;

*david.herbert@umanitoba.ca

[b]Department of Chemistry, Durham University, Durham, DH1 3LE, U.K.;

*j.a.g.williams@durham.ac.uk

ABSTRACT

The structural and photophysical properties of three sets of emissive copper complexes of the form [(*P^N*)$_2$Cu]X are presented. Here, *P^N* represents a bidentate ligand based on phenanthridine (3,4-benzoquinoline) incorporating a phosphine unit at the 4-position, of which three examples are investigated, namely 4-(diphenylphosphino)phenanthridine (**L1**), 4-(diphenylphosphino)-2-methylphenanthridine (**L2**) and 2,6-dimethyl-4-(diphenylphosphino)phenanthridine (**L3**). For each *P^N*-coordinating ligand, the corresponding homoleptic copper(I) complex (**1X**, **2X**, **3X**) has been prepared as both the hexafluorophosphate and tetraphenylborate salt (X = PF_6^- or BPh_4^-). The identity of the counterion has a profound and unexpected impact on the emission properties of the powder samples - but only for complexes of ligands bearing methyl substituents close to the metal (**3X**). The synergistic effect of combining inter-ion interactions and ligand design enabled emission tuning from orange to yellow, in the opposite (hypsochromic) direction compared to employing either strategy on its own. These effects can be attributed to differences in molecular packing, in particular to the combined impact of ligand structure and inter-ionic interactions on distortions in the excited state relative to the ground state. The results have been interpreted with the help of density functional theory (DFT) and time-dependent DFT (TD-DFT) calculations.

INTRODUCTION

The design of new emissive molecules based on low-cost and abundant metals including copper is central to increasing the sustainability of light-emitting devices, photosensitizers and imaging agents.[1-3] To fully realize the potential of luminescent Cu(I) coordination complexes, strategies to tune emission wavelengths and optimise photophysical properties, such as lifetimes and quantum yields, are critical. One prominent strategy is to use ligand design to prevent molecular distortions of tetrahedral Cu(I) complexes in the excited state that can lead to competitive non-radiative decay. For example, methylation *ortho* to the nitrogen donors in bidentate *N^N* phenanthroline frameworks has been shown to considerably reduce the apparent Stokes shift of emission and boost quantum yields for Cu(I) complexes containing such ligands, accompanied by elongation of the emission lifetimes.[4] These outcomes are associated with the influence of the methyl groups in restricting the flattening of the structure away from D_{2d} symmetry towards D_{2h}. This effect is not universal, however; for example, the impact of ligand methylation *ortho* to N-donors in Cu(I) complexes supported by 8-(diphenylphosphino)-2-methylquinoline ligands is minimal.[5] A related approach is the use of rigid media,[6] packing-effects,[7, 8] or inter-ion interactions[9-12] to control excited state reorganization. As these approaches are usually invoked independently in the literature, we were curious as to whether these tactics could be used in a complimentary fashion. Namely, in instances where the impact of one tactic on its own is limited, could combining ligand modification and solid-state effects enhance photophysical properties and potentially expand the

reach of these design strategies, similar to the recently reported synergistic activation of room temperature phosphorescence in organic materials.[13]

We report here a case study using homoleptic Cu(I) complexes of bidentate *P^N*-coordinating ligands based on a phenanthridine unit substituted at the 4-position with a diphenylphosphine moiety: **1X** (**1** = $[(\mathbf{L1})_2Cu]^+$), **2X** (**2** = $[(\mathbf{L2})_2Cu]^+$), **3X** (**3** = $[(\mathbf{L3})_2Cu]^+$), where X = PF_6^- or BPh_4^- in each case. Emission from Cu(I) complexes of both mixed *P^P*/*N^N* ligand sets[14-18] and bidentate *P^N*-coordinating ligands[19-24] has been widely explored; here, the *P^N* ligand **L1** is the parent 4-(diphenylphosphino)phenanthridine, a benzannulated analog of the phosphine/quinoline ligand utilized by Tsukuda, Tsubomura and coworkers.[5] **L2** and **L3** both incorporate a methyl substituent in the 2-position *para* to the nitrogen donor, while **L3** carries an additional methyl *ortho* to N, making it reminiscent of the *ortho*-methylated phenanthrolines mentioned above.[4] The complexes all display moderately intense orange-yellow photoluminescence in the solid-state. In investigating the photophysical properties of powder samples, we discovered a synergistic effect of counterion choice and ligand architecture modification on solid-state emission at room temperature.

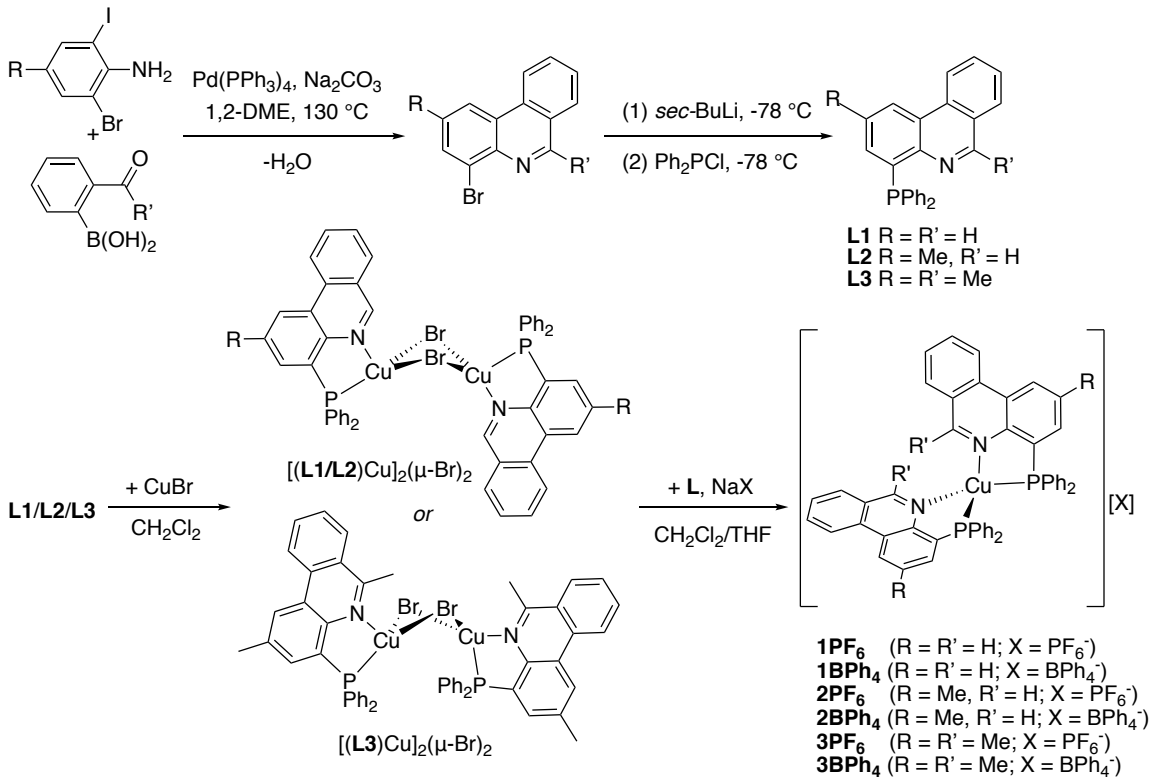

Scheme 1. Synthesis of proligands **L1**,[25] **L2**[26] and **L3** (this work) and their Cu(I) complexes.

The π-extended *P^N* donor **L3** was synthesized similarly to **L1**[25] and **L2**.[26] The tricyclic frame of the phenanthridine moiety was prepared via a one-pot, Pd-catalyzed cross-coupling/condensation of the appropriately substituted aniline with 2-acetylphenylboronic acid (Scheme 1). **L3** was then accessed via lithium-halogen exchange between 4-bromo-2,6-dimethylphenanthridine and *sec*-butyllithium, followed by quenching with Ph_2PCl. Evidence for the assembly of the phenanthridine core could be discerned in the downfield shift of the "imine-like" C_6 resonance in the $^{13}C\{^1H\}$ NMR spectrum at 157.3 ppm (*cf.* **L1**: 152.8 ppm; **L2**: 151.8 ppm).

Mixing solutions of **L1**-**L3** with suspensions of CuBr gave increasingly homogeneous orange solutions of $[(\mathbf{L})Cu]_2(\mu\text{-}Br)_2$ dimers, previously described for **L1**[25]

and **L2**.[26] Full characterization details of [(**L3**)Cu]$_2$(μ-Br)$_2$ are provided in the Supporting Information. The solid-state structure of [(**L3**)Cu]$_2$(μ-Br)$_2$ shows a bent, butterfly-like orientation to the Cu_2Br_2 sub-unit with an intermetallic distance of 2.6793(4) Å and a 'head-to-head' orientation of the two *P^N* ligands in which the nitrogen donors are on the same side of the Cu_2Br_2 core (Figure S1). In comparison, the equivalent halide-bridged dimers of [(**L1**/**L2**)Cu]$_2$(μ-X)$_2$ (X = Cl, Br, I) are all 'head-to-tail', with longer Cu-Cu distances.[25, 26] The presence of *ortho* methyl groups adjacent to the phenanthridine nitrogens thus appears to override the steric preferences of the PPh_2 units to avoid each other in the solid-state. Addition of a second equivalent of *P^N* ligand, followed by metathesis with $NaPF_6$ or $NaBPh_4$ in tetrahydrofuran, gave bright yellow/green suspensions, from which the targeted [(**L**)$_2$Cu]X salts could be isolated as light yellow solids. The Cu(I) complexes are soluble in most organic solvents, and were fully characterized in solution by multi-nuclear NMR spectroscopy, and in the solid-state by elemental analysis and single-crystal X-ray diffraction. A symmetric ligand environment was observed by NMR spectroscopy for both bound ligands in all six complexes.

In the solid-state, the cations adopt the distorted tetrahedral geometry expected of four-coordinate Cu(I) with bulky ligand sets (exemplified by the BPh_4^- series in Figure 1a; see Figure S2 for PF_6^- salts). Comparing bond distances, all complexes show very similar metal-ligand interactions (Table 1). Examining the bond angles, the differences imposed by relatively small changes in ligand sterics (i.e., replacing H with CH_3) become evident. While the bite angles (N1-Cu1-P1, for example) remain invariant as a result of the rigid sp^2 aromatic ligand backbone, the interligand angles are significantly perturbed

in moving from **1X** to **3X**. Interestingly, these differences are exacerbated in changing from PF_6^- to BPh_4^-. Thus, τ_δ metrics[27] suggest that **L1** and **L2**, bearing no additional sterically imposing substituents close to Cu, favour a distorted sawhorse geometry in their Cu(I) complexes (τ_δ ~ 0.55) when paired with a PF_6^- counterion, but enforce more of a distorted tetrahedral ligand arrangement (τ_δ ~ 0.63-0.69) as BPh_4^- salts. These distortions are caused by unequal P-Cu-P vs N-Cu-N angles, and larger dihedral angles between the Cu-P1 vectors and the plane formed by the P2-Cu-N2 sub-unit of the second *P^N* ligand compared with the equivalent dihedral angle formed by the Cu1-N1 bond/Cu-P2-N2 plane (Table S1).

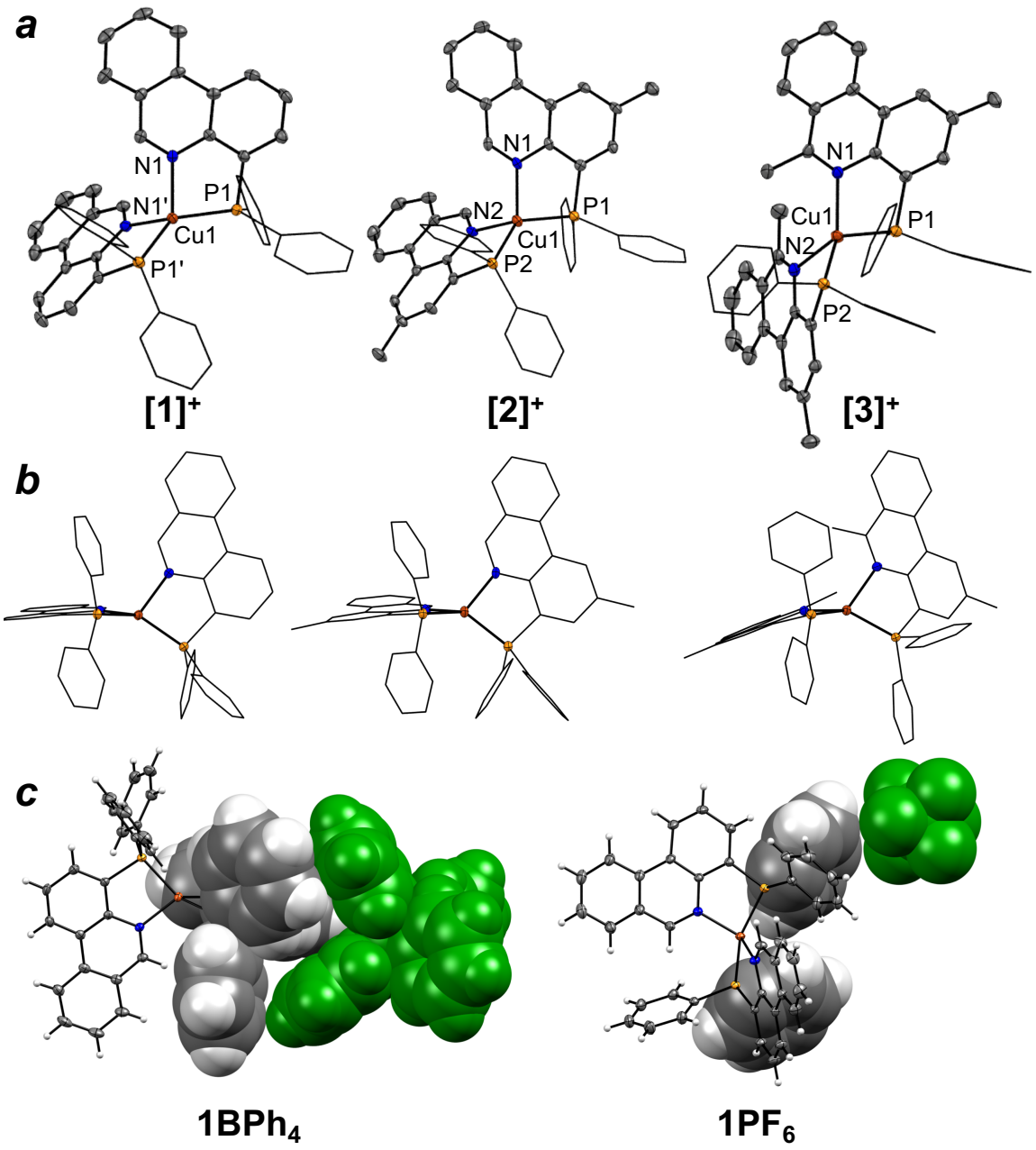

Figure 1. (a) Solid-state X-ray structures of the cationic fragments of **1BPh$_4$**, **2BPh$_4$** and **3BPh$_4$**. Hydrogen atoms, counterions and lattice-confined solvent molecules (**2BPh$_4$**) are omitted for clarity. (b) View highlighting rocking distortions from idealized tetrahedral geometry and bending of the Cu-N bond out of the phenanthridine ligand plane. (c) Partial space-filling diagrams for **1BPh$_4$** and **1PF$_6$**.

Table 1. Selected bond lengths (Å) and angles (°) for **1X**, **2X** and **3X**.

	1PF$_6$	**2PF$_6$**	**3PF$_6$**	**1BPh$_4$**	**2BPh$_4$**	**3BPh$_4$**
Cu1-N1/ Cu2-N3	2.0538(16)	2.0578(18)	2.1251(18)	2.0669(16)	2.094(3) 2.066(3)	2.0740(18)
Cu1-N2/ Cu2-N4	2.0837(15)		2.0951(19)		2.061(3) 2.073(3)	2.1222(18)
Cu1-P1/ Cu2-P3	2.2195(5)	2.2016(6)	2.2162(6)	2.2328(5)	2.2041(10) 2.2229(10)	2.2527(6)
Cu1-P2/ Cu2-P4	2.2115(5)		2.2265(6)		2.2222(10) 2.2197(10)	2.2251(6)
N1-Cu1-N2/ N3-Cu2-N4	109.20(6)	100.19(10)	118.93(7)	105.46(9)	101.40(11) 105.94(11)	123.78(7)
P1-Cu1-P2/ P3-Cu2-P4	145.49(2)	146.99(4)	133.23(2)	136.73(3)	131.49(4) 137.17(4)	126.15(2)
N1-Cu1-P1/ N3-Cu2-P3	87.31(5)	86.83(5)	85.63(5)	87.04(5)	86.70(8) 86.14(8)	87.92(5)
N2-Cu1-P2 N4-Cu2-P4	86.34(4)		86.65(5)		86.59(8) 86.79(8)	85.02(5)
N1-Cu1-P2/ N3-Cu2-P4	116.41(5)	114.83(5)	114.67(5)	119.87(5)	117.95(8) 116.76(8)	129.20(5)
N2-Cu1-P1/ N4-Cu2-P3	110.26(5)		121.21(5)		131.48(8) 123.11(8)	106.63(5)
τ_δ[a]	0.56	0.54	0.68	0.64	0.69, 0.63	0.72

[a] $\tau_\delta = \delta*[360-(\alpha+\beta)]/141$, where $\delta = \beta/\alpha$, the ratio of the second largest (β) to largest (α) angle.[27]

The inequivalence of these angles is smallest in **3X**. In particular, the N-Cu-N angles are much larger (and closer in magnitude to the P-Cu-P angles) for **3X**, owing to the presence of the *ortho* methyl groups. Increased steric demand close to the donor nitrogen in **L3** thus disfavours distortion from an idealized tetrahedral geometry for both BPh_4 and PF_6 salts. More pronounced are rocking distortions[4] (Figure 1b), as well as the marked bending of the Cu-N bond out of plane with the phenanthridine ligand in **3X**; the dihedral angle of the Cu-N vector with the plane formed by the phenanthridine moiety reaches 21° in **3X**, compared with an arrangement much closer to coplanarity in **1X**/**2X** (~0-5°). Comparing **3BPh$_4$** and **3PF$_6$**, the N-Cu-N angles are similar, but the P-Cu-P angles are much smaller in **3BPh$_4$**. Space-filling diagrams reveal that these geometric constraints result from more intimate inter-ion contacts for the BPh_4^- salts (Figure 1c).

Absorption spectra of the Cu(I) complexes in CH_2Cl_2 solution at room temperature (Figure S3) show strong absorbance in the UV (250-300 nm; $\varepsilon \sim 35 \times 10^3$ $M^{-1}cm^{-1}$), with two distinct but weaker bands at ~350 nm that also appear in the spectra of the proligands (Figure S4). The major difference between the absorption profile of the ligands and their Cu(I) complexes is the longer wavelength tail observed for the complexes, attributable to relatively weak, spin-allowed, charge-transfer transitions (^{1}CT) in which the phenanthridine heterocycle serves as the CT acceptor. By analogy to homoleptic $[(N\text{^}N)_2Cu]^+$ complexes,[28] we assign these as metal-to-ligand charge-transfer (^{1}MLCT) in character, the donor orbitals being predominantly of metal-based *d* character with participation from the phosphine-metal bonding pairs. Close examination of the peaks around ~341 and ~357 nm revealed only a small bathochromic shift for all BPh_4^- complexes, with the sets of spectra otherwise indistinguishable.

Electrochemical analysis of all three complexes showed irreversible redox events at similar potentials vs $FcH^{0/+}$ (FcH = $(\eta^5\text{-}C_5H_5)_2Fe$; Figure S5). Comparing the onset of the reduction events for **1**-**3**, a slight cathodic shift is observed with alkylation of the phenanthridinyl unit as the addition of an inductively donating methyl group renders the complexes harder to reduce (**1PF$_6$** ~ -2.14 V, **2PF$_6$** ~ -2.22 and **3PF$_6$** ~ -2.36 V vs $FcH^{0/+}$). This impact of alkylation is regio-specific: alkylation at the 6-position in **3PF$_6$** results in a more negatively shifted reduction potential relative to **1PF$_6$**, compared to alkylation at the 2-position in **2PF$_6$**. This is likely a consequence of the LUMO being structured with lobes localized at the C=N sub-unit in the 6-position (Figure S40). The Cu(I/II) oxidation event is affected according to the same trend as the reduction peaks but in the opposite

direction, with a slight anodic shift upon alkylation that is also regiospecific (**1PF$_6$** ~0.76 V, **2PF$_6$** ~0.74 and **3PF$_6$** ~0.69 vs $FcH^{0/+}$). As a result of these offsetting effects, the separation between oxidation and reduction events measured by electrochemistry is more or less equivalent for all three complexes. Using these separations to estimate the HOMO-LUMO gap[29] shows that all complexes thus fall within a relatively narrow spread of 150 mV (Table S2), consistent with the nearly isoenergetic lowest energy peaks observed by absorption spectroscopy. TD-DFT vertical absorption energies and the HOMO-LUMO gap estimated by DFT-determined frontier orbital energies are accordingly very similar for the three cations **1**$^+$, **2**$^+$ and **3**$^+$ (Table S5).

The complexes are not emissive in solution at ambient temperature, even with rigorous exclusion of oxygen. In contrast, powdered samples are brightly luminescent to the eye when observed under long-wavelength UV irradiation, glowing bright yellow to orange in colour (Figure S6). The emission of the samples was therefore studied in the solid state at ambient temperature. An integrating sphere was used to evaluate photoluminescence quantum yields (Φ_{lum}) under continuous-wave excitation, with pulsed laser diode excitation to measure the corresponding luminescence lifetimes (τ; Table 2). Broad, featureless emission peaks are observed, consistent with MLCT character to the emissive state,[28, 30] with maxima between 584 and 647 nm (Figure 2). Quantum yields hover mostly around 2%, but are significantly higher for **3BPh$_4$**. The lifetimes are roughly of the order of 1 μs, with some variation; **3BPh$_4$** is again notable in that it displays a significantly longer lifetime. PF_6^- salts of Cu(I) complexes of bidentate *P^N* ligands incorporating smaller quinolinyl π-systems, but that are otherwise directly analogous to

1PF$_6$ and **3PF$_6$**, both show broad emission centred at 640 nm despite ligand *ortho*-alkylation, with lifetimes of 0.33 and 1.0 μs, respectively.[5] In comparison, the emission maximum of **1PF$_6$** at room temperature is blue-shifted by 12 nm compared to **2PF$_6$**, and 22 nm compared to **3PF$_6$**. A similar trend in the apparent Stokes shift was observed for emission from [(**L**)Cu]$_2$(μ-I)$_2$ dimers, with a hypsochromic shift for emission from the parent [(**L1**)Cu]$_2$(μ-I)$_2$ relative to the alkylated [(**L2**)Cu]$_2$(μ-I)$_2$.[26] While this same trend holds for room temperature emission from **1BPh$_4$** (λ_{em} = 618 nm) and **2BPh$_4$** (λ_{em} = 647 nm), a considerable hypsochromic shift in the *opposite* direction is seen for **3BPh$_4$** (λ_{em} = 584 nm), consistent with trends in emission from [(*N^N*)(*P^P*)Cu(I)]$^+$ complexes with *ortho*-methylated phenanthroline ligands.[17] The anticipated effect of ligand substitution *ortho* to the coordinating nitrogen, *not* observed for the set of PF_6^- salts, is therefore "turned on" for **3X** by changing the counterion to BPh_4^-. Comparing each set of ion pairs (**LX**, X = PF_6^- vs BPh_4^-), changing the counterion from PF_6^- to BPh_4^- results in a red shift of the emission maximum by 11 and 28 nm for **1X** and **2X**, respectively, but a *blue* shift of 45 nm for **3X**. Combining ligand modification (increased sterics next to N donors; Figure 1b) and counterion effects (increased inter-ion interactions; Figure 1c) thus impacts room-temperature emission in a synergistic fashion for these complexes, in a different manner from each strategy on its own.

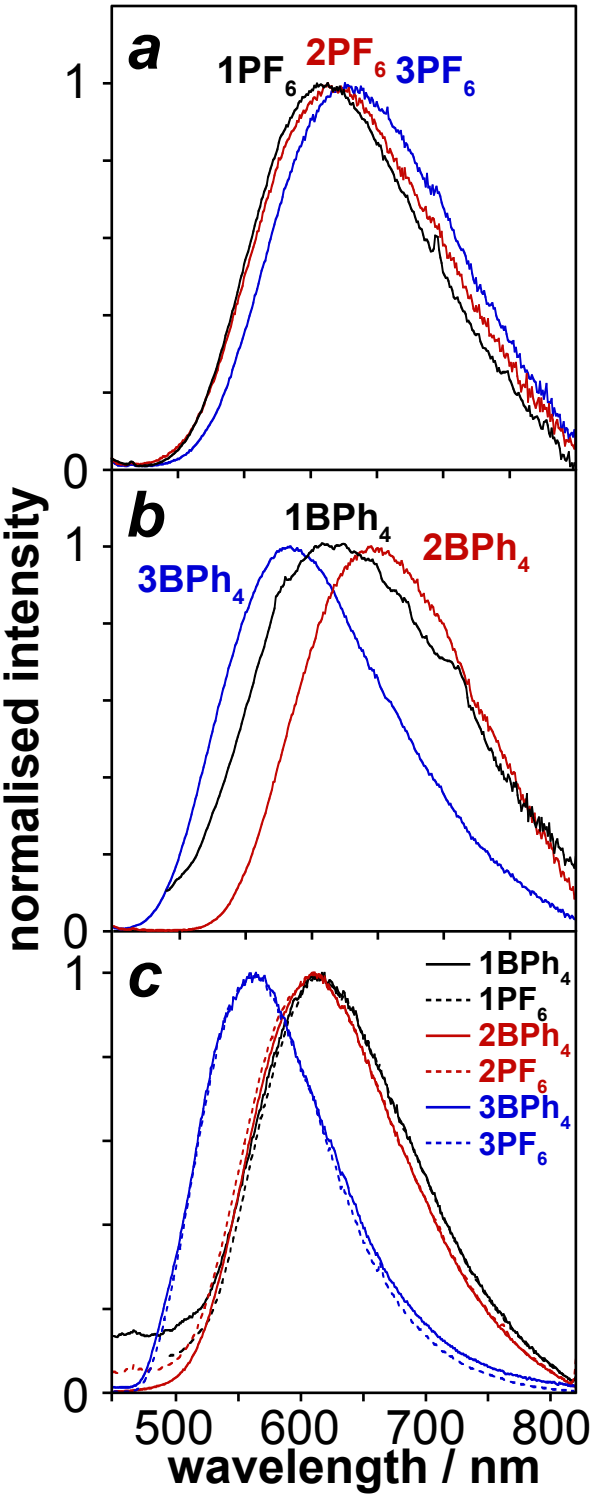

Figure 2. Emission spectra of **1X**, **2X** and **3X** in the solid-state at 298 ± 3 K λ_{ex} = 425 nm, where X = *(a)* PF_6^- or *(b)* BPh_4^- and *(c)* in dilute EPA glass at 77 K, λ_{ex} = 370 nm.

Table 2. Emission data for **1X**, **2X** and **3X** in the solid state at 298 ± 1 K and in dilute EPA glass at 77 K.

	Emission, solid state 298±1 K			Emission, EPA glass 77 K[c]	
	λ_{max}[a] / nm	Φ_{lum}[a] × 10^2	τ[b] / ns	λ_{max} / nm	τ[d] / μs
1PF$_6$	607	2.4	2100	615	51, 144 (43/56)
2PF$_6$	619	0.80	1900	611	39, 150 (28/72)
3PF$_6$	629	1.7	1300	564	740
1BPh$_4$	618	2.9	710	615	47, 134 (35/65)
2BPh$_4$	647	2.0	840	611	48, 160 (28/72)
3BPh$_4$	584	8.9	7400	564	730

(a) Recorded using an integrating sphere, λ_{ex} = 425 nm. *(b)* Measured by time-correlated single-photon counting, λ_{ex} = 425 nm. *(c)* EPA = diethyl ether/isopentane/ethanol (2:2:1 v/v). *(d)* Measured by multichannel scaling, λ_{ex} = 370 nm. Where two values are given, the decay follows biexponential kinetics with relative magnitudes of the two components in parenthesis.

Attributing this effect to enhanced molecular rigidity is supported by the low temperature emission spectra (Figure 2c). In a frozen glass of EPA at 77 K, complexes **1X** and **2X** display orange/red luminescence whilst the brighter luminescence of **3X** is green-yellow to the eye (EPA = diethyl ether / isopentane / ethanol, 2:2:1 v/v). The corresponding emission spectra are broad and structureless, and highlight a substantial blue shift of **3X** relative to **1X** and **2X** (whose emission maxima are similar to one another) regardless of counterion. The substantial hypsochromic shift of the phosphorescence of **3X** relative to the other complexes at low temperature, despite the absorption spectra being so similar for all complexes, is consistent with the steric influence of the *ortho* methyl groups inhibiting attainment of a geometry that most stabilises the triplet state. At low temperature, *ortho* methylation clearly has a large impact on structural reorganization, whereas methylation *para* to nitrogen (i.e., in **L2**) does not, consistent with Cu(I) complexes of *ortho*-methylated phenanthroline *N^N* ligands.[4, 6] The timescale

of low temperature luminescence is long, indicative of phosphorescence from a triplet state: **3PF$_6$** and **3BPh$_4$** have identical lifetimes within the uncertainty on the measurement (740 and 730 μs, respectively). The emission of complexes **1X** and **2X** is shorter, showing biexponential decay, and fitting to a major component of about 150 μs and a minor of around 50 μs in each case. The origin of the biexponential nature of the decay is unclear. It may be due to inhomogeneities owing to poor solubility in the EPA glass at low temperature. However, what is clear is that the formally forbidden $T_1 \rightarrow S_0$ emission is evidently promoted by the Cu(I) centre, as the phosphorescence lifetimes of the corresponding free *P^N* ligands are of the order of hundreds of *milliseconds* (τ = 240, 310, and 530 ms for **L1**, **L2**, and **L3**, respectively; Figure S7). The temporal decay of their emission is easily visible to the naked eye.

To further investigate the origin of this effect, we optimized gas-phase geometries of the isolated cations in both the ground state (S_0) and first triplet excited state (T_1) using DFT, and probed the nature of the optical transitions with TD-DFT. Consistent with the absorption spectra, the vertical transitions to the lowest lying singlet states are very similar in energy for all three cations (Table S5). The lowest energy excitations are HOMO→LUMO/HOMO-1→LUMO+1 in character, as can be visualized in the electron/hole maps in Figure S41. Re-optimizing the geometry of each ground state as a triplet gave the geometry and free energy of the lowest lying triplet states (T_1). In the T_1 excited state, all three cations show elongation of Cu-P distances, which is most pronounced for **1$^+$** (Table S3). This is consistent with participation of filled Cu-P σ-bonding orbitals in the MLCT excitation to vacant π^* acceptor orbitals on phenanthridine. The

trend observed in the low temperature emission spectra could be reproduced computationally; TD-DFT calculated phosphorescence energies for $\mathbf{1}^+$ and $\mathbf{2}^+$ are nearly equivalent, and smaller than that calculated for $\mathbf{3}^+$. A slightly larger singlet-triplet gap was calculated for $\mathbf{2}^+$ compared to $\mathbf{1}^+$, whilst $\mathbf{3}^+$ has the smallest calculated singlet-triplet gap and smallest reorganization energy.[31] The lowest lying triplet state of $\mathbf{3}^+$ is higher in energy than for $\mathbf{1}^+/\mathbf{2}^+$ and incurs the least structural reorganization upon relaxation to the ground state.

So why is this predicted impact only observed at room temperature for the BPh_4^- complexes? The most pronounced structural change is to the coordination geometry of the four-coordinate Cu centre. The three optimized S_0 structures have τ_δ metrics of 0.57 ($\mathbf{1}^+$), 0.57 ($\mathbf{2}^+$) and 0.71 ($\mathbf{3}^+$; Table S4), which align well with the τ_δ metrics and distorted sawhorse geometries of the PF_6^- salts (Table 1). In the T_1 state, a distinct distortion towards true sawhorse geometry is accompanied by a reduction in τ_δ to 0.44 ($\mathbf{1}^+$), 0.44 ($\mathbf{2}^+$) and 0.56 ($\mathbf{3}^+$). In addition, for $\mathbf{1}^+/\mathbf{2}^+$ the P-Cu-P angles compress significantly from 144° in the ground state to 109° in the first excited triplet state (Table S3). The same angle in the more sterically encumbered $\mathbf{3}^+$ is also made more acute in the excited state (S_0: 131° vs. T_1: 108°), but as this angle is tighter in the ground state already, the change is not as drastic. The N-Cu-N angles are relatively invariant for all three complexes, constricting by only a few degrees for $\mathbf{1}^+/\mathbf{2}^+$ (S_0: 109° vs. T_1: 106°) and relaxing slightly for $\mathbf{3}^+$ (S_0: 119° vs. T_1: 121°). Thus, inclusion of 6-position methyl groups on its own is not enough to prevent significant reorganization in the emissive states at room temperature. As a result, emission from $\mathbf{1PF_6}$, $\mathbf{2PF_6}$ and $\mathbf{3PF_6}$ is most strongly affected by the increased degrees of

freedom from an added alkyl substituent, which red-shifts emission to lower energy. Replacing PF_6^- with BPh_4^- leads to closer inter-ion contacts in the solid-state (*cf.* Figure 1c). As can be seen in Figure 3, to minimize motion of the large phenanthridinyl moiety, the PPh_2 fragment twists substantially in the T_1 geometry, which is hampered by the presence of the BPh_4^- ion. This twisting is not sufficiently inhibited by 6-alkylation alone (e.g., comparing **1PF$_6$** and **3PF$_6$**). Similarly, for **1X** and **2X**, the presence of close inter-ion interactions in the *absence* of 6-alkylation is also insufficient for preventing significant reorganization: the BPh_4^- and PF_6^- salts both apparently undergo considerable distortions, likely through changes to τ_δ ($\Delta\tau_\delta$). The larger distortions result in lower energy emission. Only when increased ligand sterics (6-position alkylation) is combined with enhanced inter-ion interactions is a boost in quantum yield of **3BPh$_4$** via reduction of non-radiative decay rates observed, along with a substantial blue-shift in the wavelength of emission even at ambient temperature. Thus, as seen in the case of **3X**, combining close inter-ion interactions and ligand design can amplify photophysical properties in a synergistic fashion.

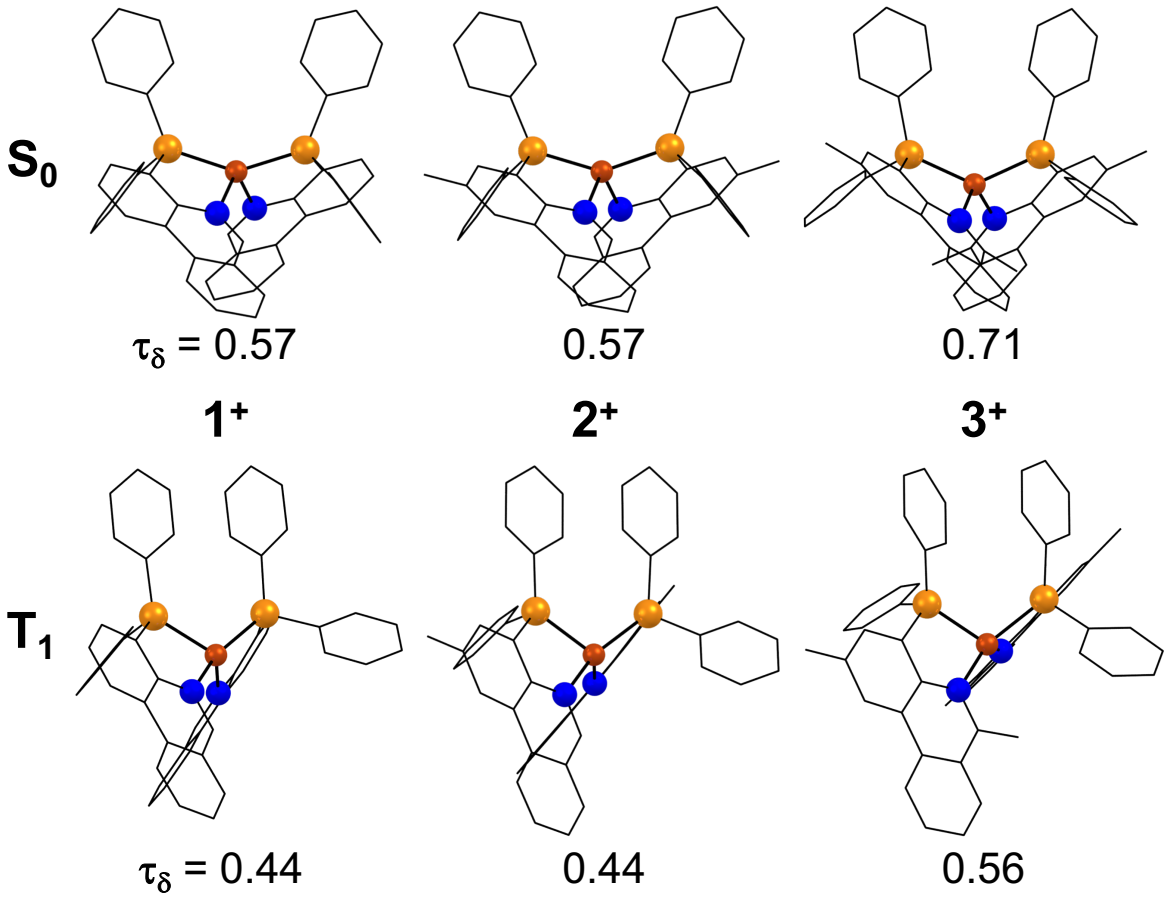

Figure 3. Optimized geometries and τ_δ[27] metrics of the ground-state (S_0) and first excited triplet state (T_1) of **1**$^+$, **2**$^+$ and **3**$^+$.

In conclusion, we present a case study wherein exploiting the synergy between ligand modification (in this case, *P^N* ligand *ortho* methylation) and inter-ion interactions can tune emission from orange-red to quite bright, yellow (λ_{max} shifting from 647 to 584 nm) in Cu(I) complexes of bidentate, benzannulated *P^N* ligands. Yellow-emitting Cu(I) complexes are relatively rare,[32-38] despite yellow being a key component for achieving white light emission in light emitting devices.[39] The applicability of this method for amplifying ligand effects through choice of counterion to other phosphorescent emitters is currently underway.

ASSOCIATED CONTENT

Supporting Information. Multi-nuclear NMR spectra of all new compounds; additional UV-vis absorption and emission spectra; details of computational methods; combined crystallographic information file containing all X-ray data. CCDC 1872863-1872869 contain the supplementary crystallographic data for this paper. The data can be obtained free of charge from The Cambridge Crystallographic Data Centre via www.ccdc.cam.ac.uk/structures.

The following files are available free of charge:

Supporting Information File (PDF)

Combined Crystallographic Information File (CIF)

AUTHOR INFORMATION

Corresponding Authors

david.herbert@umanitoba.ca, j.a.g.williams@durham.ac.uk

ORCID

Rajarshi Mondal: 0000-0002-6819-6690

Issiah B. Lozada: 0000-0002-1689-2918

Rebecca L. Davis: 0000-0002-0679-6025

J. A. Gareth Williams: 0000-0002-4688-3000

David E. Herbert: 0000-0001-8190-2468

Author Contributions

The manuscript was written through contributions of all authors. All authors have given approval to the final version of the manuscript.

Funding Sources

The following sources are gratefully acknowledged: Natural Sciences Engineering Research Council of Canada for a Discovery Grant to DEH (RGPIN-2014-03733); the Canadian Foundation for Innovation and Research Manitoba for an award in support of an X-ray diffractometer (CFI #32146); the University of Manitoba for start-up funding (DEH) and GETS support (RM, IBML). The Association of Commonwealth Universities (ACU) is thanked for a University of Manitoba Titular Fellowship (2016–17) to JAGW.

ACKNOWLEDGMENTS

We are grateful to Prof. Mazdak Khajehpour for access to a UV-Vis spectrometer.

REFERENCES

1. B. Bozic-Weber, E. C. Constable and C. E. Housecroft, *Coord. Chem. Rev.*, 2013, **257**, 3089-3106.
2. C. E. Housecroft and E. C. Constable, *Chem. Soc. Rev.*, 2015, **44**, 8386-8398.
3. E. Cariati, E. Lucenti, C. Botta, U. Giovanella, D. Marinotto and S. Righetto, *Coord. Chem. Rev.*, 2016, **306**, 566-614.
4. C. T. Cunningham, J. J. Moore, K. L. H. Cunningham, P. E. Fanwick and D. R. McMillin, *Inorg. Chem.*, 2000, **39**, 3638-3644.
5. T. Tsukuda, C. Nishigata, K. Arai and T. Tsubomura, *Polyhedron*, 2009, **28**, 7-12.

6. R. M. Everly, R. Ziessel, J. Suffert and D. R. McMillin, *Inorg. Chem.*, 1991, **30**, 559-561.
7. L. Zhang, B. Li and Z. Su, *Langmuir*, 2009, **25**, 2068-2074.
8. D. Volz, M. Nieger, J. Friedrichs, T. Baumann and S. Brase, *Langmuir*, 2013, **29**, 3034-3044.
9. H. Yersin, H. Otto and G. Gliemann, *Theo. Chim. Acta*, 1974, **33**, 63-78.
10. T. Gneuss, M. J. Leitl, L. H. Finger, H. Yersin and J. Sundermeyer, *Dalton Trans.*, 2015, **44**, 20045-20055.
11. B. Hupp, J. Nitsch, T. Schmitt, R. Bertermann, K. Edkins, F. Hirsch, I. Fischer, M. Auth, A. Sperlich and A. Steffen, *Angew. Chem., Int. Ed.*, 2018, **57**, 13671-13675.
12. Y. Ma, Y. Dong, P. She, S. Liu, M. Xie, Y. Yu, Y. Li, Q. Zhao and W. Huang, *Adv. Opt. Mater.*, 2018, **6**, 1801065.
13. X. Kong, X. Wang, H. Cheng, Y. Zhao and W. Shi, *J. Mater. Chem. C*, 2019, **7**, 230-236.
14. M. T. Buckner, T. G. Matthews, F. E. Lytle and D. R. McMillin, *J. Am. Chem. Soc.*, 1979, **101**, 5846-5848.
15. A. A. Del Paggio and D. R. McMillin, *Inorg. Chem.*, 1983, **22**, 691-692.
16. C. E. A. Palmer and D. R. McMillin, *Inorg. Chem.*, 1987, **26**, 3837-3840.
17. D. G. Cuttell, S.-M. Kuang, P. E. Fanwick, D. R. McMillin and R. A. Walton, *J. Am. Chem. Soc.*, 2002, **124**, 6-7.
18. S.-M. Kuang, D. G. Cuttell, D. R. McMillin, P. E. Fanwick and R. A. Walton, *Inorg. Chem.*, 2002, **41**, 3313-3322.
19. S. B. Harkins and J. C. Peters, *J. Am. Chem. Soc.*, 2005, **127**, 2030-2031.
20. A. J. M. Miller, J. L. Dempsey and J. C. Peters, *Inorg. Chem.*, 2007, **46**, 7244-7246.
21. N. P. Mankad, S. B. Harkins, W. E. Antholine and J. C. Peters, *Inorg. Chem.*, 2009, **48**, 7026-7032.
22. J. C. Deaton, S. C. Switalski, D. Y. Kondakov, R. H. Young, T. D. Pawlik, D. J. Giesen, S. B. Harkins, A. J. M. Miller, S. F. Mickenberg and J. C. Peters, *J. Am. Chem. Soc.*, 2010, **132**, 9499-9508.
23. K. J. Lotito and J. C. Peters, *Chem. Commun.*, 2010, **46**, 3690-3692.
24. T. McCormick, W.-L. Jia and S. Wang, *Inorg. Chem.*, 2006, **45**, 147-155.
25. R. Mondal, P. K. Giesbrecht and D. E. Herbert, *Polyhedron*, 2016, **108**, 156-162.
26. R. Mondal, I. B. Lozada, R. L. Davis, J. A. G. Williams and D. E. Herbert, *Inorg. Chem.*, 2018, **57**, 4966-4978.
27. M. H. Reineke, M. D. Sampson, A. L. Rheingold and C. P. Kubiak, *Inorg. Chem.*, 2015, **54**, 3211-3217.
28. N. Armaroli, G. Accorsi, F. Cardinali and A. Listorti, in *Photochemistry and Photophysics of Coordination Compounds I*, eds. V. Balzani and S. Campagna, Springer-Verlag Berlin, Berlin, 2007, vol. 280, pp. 69-115.
29. B. W. D'Andrade, S. Datta, S. R. Forrest, P. Djurovich, E. Polikarpov and M. E. Thompson, *Org. Electron.*, 2005, **6**, 11-20.
30. R. Czerwieniec, M. J. Leitl, H. H. H. Homeier and H. Yersin, *Coord. Chem. Rev.*, 2016, **325**, 2-28.

31. H. Uoyama, K. Goushi, K. Shizu, H. Nomura and C. Adachi, *Nature*, 2012, **492**, 234-238.
32. Q. Benito, X. F. Le Goff, S. Maron, A. Fargues, A. Garcia, C. Martineau, F. Taulelle, S. Kahlal, T. Gacoin, J.-P. Boilot and S. Perruchas, *J. Am. Chem. Soc.*, 2014, **136**, 11311-11320.
33. S.-Q. Bai, D. Kai, K. L. Ke, M. Lin, L. Jiang, Y. Jiang, D. J. Young, X. J. Loh, X. Li and T. S. A. Hor, *ChemPlusChem*, 2015, **80**, 1235-1240.
34. W. Chai, M. Hong, L. Song, G. Jia, H. Shi, J. Guo, K. Shu, B. Guo, Y. Zhang, W. You and X. Chen, *Inorg. Chem.*, 2015, **54**, 4200-4207.
35. C. Wang, Z. Hu, S. Xu, Y. Wang, Z. Zhao, Z. Wang and Y. Cui, *Nanotechnology*, 2015, **26**, 1-6.
36. J. Zhang, C. Duan, C. Han, H. Yang, Y. Wei and H. Xu, *Adv. Mater.*, 2016, **28**, 5975-5979.
37. G. Attilio Ardizzoia, S. Brenna, F. Civati, V. Colombo and A. Sironi, *CrystEngComm*, 2017, **19**, 6020-6027.
38. J. Feng, Y. Chen, Y. Han, J. Liu, S. Ma, H. Zhang and X. Chen, *ACS Omega*, 2017, **2**, 9109-9117.
39. M. Y. Wong and E. Zysman-Colman, *Adv. Mater.*, 2017, **29**, 1605444.